Toxicology in Vitro 108 (2025) 106105

Contents lists available at ScienceDirect

Toxicology in Vitro

journal homepage: www.elsevier.com/locate/toxinvit

E171-induced toxicity in human iPSC-derived colon organoids: Effects on cell viability, ROS generation, DNA damage, and gene expression changes

Nicolaj S. Bischoff [a,*], Anna K. Undas [b], Marcel van Herwijnen [a], Marcha Verheijen [a], Jacco J. Briedé [a], Simone G. van Breda [a], Dick T.H.M. Sijm [c,d], Theo M. de Kok [a]

[a] Department of Translational Genomics, GROW Research Institute for Oncology and Reproduction, Maastricht University Medical Centre, 6229 ER Maastricht, the Netherlands
[b] Wageningen Food Safety Research (WFSR), Wageningen University & Research, 6708 WB Wageningen, the Netherlands
[c] Department of Pharmacology and Toxicology, Maastricht University, 6229 ER Maastricht, the Netherlands
[d] Office of Risk Assessment and Research, Netherlands Food and Consumer Product Safety Authority, PO Box 43006, 3540 AA Utrecht, the Netherlands

ARTICLE INFO

Editor: Martin Leonard

Keywords:
E171
Titanium dioxide
DNA damage
RNA sequencing
Food safety

ABSTRACT

Food-grade titanium dioxide (E171) is a widely used food additive with debated safety, particularly regarding its genotoxic effects. This study assessed the dose-dependent toxicity of E171 in human induced pluripotent stem cell (iPSC)-derived colon organoids. Organoids were exposed to E171 (0.1–1000 μg/mL) for 24 h, and effects on cell viability, reactive oxygen species (ROS) generation, DNA damage, and gene expression were evaluated.

Results showed no impact on cell viability but a dose-dependent increase in ROS formation, peaking at 1000 μg/mL. Electrospin Resonance Spectroscopy (ESR) showed a dose-dependent increase in ROS, with increased E171 concentrations. The alkaline comet assay revealed significant DNA damage from 100 μg/mL, with oxidative DNA damage detected at 10 μg/mL using formamidopyrimidine DNA glycosylase (FPG). RNA sequencing identified differentially expressed genes (DEGs) at 100 and 250 μg/mL, linked to translational activity, signal transduction, and DNA damage repair. Gene set enrichment analysis (GSEA) indicated activation of ribosome, chemical carcinogenesis–ROS, and metabolic pathways (carbon metabolism, glycolysis), while key regulatory pathways (Wnt, MAPK, PI3K-Akt) were suppressed.

These findings suggest that E171 induces oxidative stress and DNA damage, modulating transcriptomic pathways associated with metabolism, proliferation, and cancer. Further research is necessary to determine its long-term effects on human gastrointestinal health.

1. Introduction

Titanium dioxide (TiO_2) is a white food coloring and opacifying agent known as E171 in the European Union and Asia and INS171 in North America. E171 is widely used in various products, including candies, confectionaries, sauces, and pharmaceuticals (Weir et al., 2012; Bischoff et al., 2020). Its physicochemical properties, such as high refractive index and brightness, have made it a preferred additive for enhancing the aesthetic appeal of products (Weir et al., 2012; Winkler et al., 2018). E171 has been considered safe for oral intake, however, a growing body of evidence indicates that E171 shows genotoxic effects and has pro-inflammatory properties, rendering it potentially unsafe

Abbreviations: AU, Arbitrary Units; AOM, Azoxymethane; ATP, Adenine Triphosphate; BCL, Binary Base Call; CI, Confidence Interval; CMH, 1-Hydroxy-3-methoxycarbonyl-2,2,5,5-tetramethyl pyrrolidine; CRC, Colorectal Cancer; DEG, Differentially Expressed Gene; DLS, Dynamic Light Scattering; DMSO, Dimethyl sulfoxide; DNA, Deoxyribonucleic Acid; DSS, Dextran Sulfate Sodium; EC, European Commission; ECM, Extracellular Matrix; EDTA, Ethylenediaminetetraacetic acid; ESR, Electron spin Resonance; FDA, Federal Drug Authority; FDR, False Discovery Rate; FPG, Formamidopyrimidine DNA Glycosylase; GPCR, G-Protein coupled receptor; GSEA, Gene Set Enrichment Analysis; HD, Hydrodynamic Diameter; HEPES, N-2-hydroxyethylpiperazine-N-2-ethane sulfonic acid; iPSC, induced Pluripotent Stem Cells; LMP, Low Melting Point; MOET, Multi Ontology Enrichment Tool; MQ, MilliQ water; NaCl, Natrium Chloride; NaOH, Natrium hydroxide; NES, Normalized enrichment score; ODR, Organoid Dissociation Reagent; ORA, Over Representation Analysis; PBS, Phosphate Buffer Saline; PDI, Poly Dispersion Index; PENSTREP, Penicillin Streptomycin; RIN, RNA integrity number; RNA, Ribonucleic acid; ROS, Reactive Oxygen Species; RSEM, RNA-Seq by Expectation-Maximization; TEM, Transmission Electron Microscopy; TiO_2, Titanium Dioxide; USA, United States of America; VC, Vehicle Control.

* Corresponding author.
E-mail address: n.bischoff@maastrichtuniversity.nl (N.S. Bischoff).

https://doi.org/10.1016/j.tiv.2025.106105
Received 8 February 2025; Received in revised form 14 June 2025; Accepted 6 July 2025
Available online 10 July 2025

(Younes et al., 2021).

The increasing evidence on potential genotoxic effects ultimately led to the ban of E171 as a food additive within the European Union (EU) as of August 2022 and its removal from Annexes II and III of Regulation (EC) No 1333/2008 (Commission Regulation 2022/63) (EEA, 2022). Despite these concerns and regulatory actions, other views exist. Regulatory agencies in Canada (Health Canada) and the USA (Food and Drug Administration, FDA) maintained their position that E171 is safe at the currently allowed dose levels (Canada, 2023; *Titanium Dioxide as a Color Additive in Foods*, 2024). They argue that its interaction with food and the digestive tract may mitigate its adverse effects, as demonstrated in in vitro and animal models, through increased particle aggregation within the food matrix and along the gastrointestinal (GI) route (Blevins et al., 2019; Dudefoi et al., 2021). When E171 was administered to rats via feed, it did not affect the immune system or inflammatory markers, leading to contradicting results compared with a similar in vivo study that administered the E171 via oral gavage (Blevins et al., 2019; Bettini et al., 2017). Furthermore, studies that only assess the effects of TiO_2 nanoparticles (< 100 nm) following high-frequency dispersion protocols do not adequately represent the situation in humans and overestimate the exposure to the nanoparticles (Canada, 2023; *Titanium Dioxide as a Color Additive in Foods*, 2024).

Initial concerns about adverse effects of oral E171 exposure have been raised by animal studies indicating a potential role in colorectal cancer (CRC) development and progression (Bettini et al., 2017; Urrutia-Ortega et al., 2016). Research utilizing rodent models, particularly models such as azoxymethane (AOM) and dextran sodium sulfate (DSS) to induce colitis-associated cancer, demonstrated an upregulation of tumor progression markers such as COX2, Ki67, and beta-catenin (Urrutia-Ortega et al., 2016). The same study also observed dysplastic changes in the colonic epithelium, including a reduction of goblet cell numbers (Urrutia-Ortega et al., 2016). Additionally, E171 has been linked to the development of aberrant crypt foci, preneoplastic lesions in the colon, and immune system alterations, as indicated by shifts in Th1/Th17 balance (Bettini et al., 2017). Toxicogenomic studies corroborate these findings, showing transcriptional changes in colonic tissues in mice and human colon carcinoma cell lines indicative of early markers of CRC development, mainly through G-protein-coupled receptor (GPCR) signaling and DNA damage repair (Proquin et al., 2018a; Proquin et al., 2018b; Bischoff et al., 2022; Proquin et al., 2019). Furthermore, a recent human study by Putra et al. (2024) assessed stool TiO_2 levels via inductively coupled plasma–mass spectrometry (spICP-MS) and markers for gastrointestinal health. It showed that higher levels of TiO_2 in human feces were associated with increased biomarkers for gut permeability (alpha-1 antitrypsin) and gut inflammation (calprotectin) in healthy young adults (Putra et al., 2024).

The first endeavors of using human biopsy-derived colon organoids or murine gut organoids for the risk assessment of TiO_2 have been made by Park et al. (2020) and Malaise et al. (2024) (Park et al., 2020; Malaise et al., 2024). Human biopsy-derived colon organoids were exposed to TiO_2 nanoparticles for 48 h, which showed an IC50 value of 12.5 mM and revealed increased protein expression of Bax/Bcl-2 and Cytochrome-C of 2.6-fold and 1.6-fold, respectively (Park et al., 2020). Gene expression analysis using PCR arrays revealed the modulation of 22 out of 84 tested key genes relating to insulin precursors and caspase activity (Park et al., 2020). Malaise et al. (2024) showed that enteroid-derived monolayers derived from murine intestinal organoids were a suitable model for assessing potential E171-related toxicity. The results showed E171-induced apoptosis, dose-dependent genotoxicity, and gene expression alterations related to decreased antimicrobial peptides and tight junction function following 24 h of exposure (Malaise et al., 2024).

The advent of 3D cell culture technologies, particularly the utilization of human induced pluripotent stem cell (iPSC) derived organoids, represents a potential paradigm shift in toxicological research (Kim et al., 2020; Augustyniak et al., 2019). Unlike conventional 2D cell culture systems, which offer a limited approximation of in vivo conditions, 3D organoids closely mimic human tissue architectural and functional complexity (Augustyniak et al., 2019). The 3dGRO™ Human iPSC Derived Colon Organoids provide a compelling example of this technological advance. Derived from integration-free human iPSCs using the Simplicon RNA reprogramming technology, these organoids express key colon-specific markers and replicate the physiological characteristics of the gastrointestinal system. The benefits of 3D iPSC-derived colon organoids in toxicological studies are multifaceted (Nikonorova et al., 2023). These organoids maintain the intestinal epithelium's intricate cellular architecture and function, enabling a more accurate simulation of human gastrointestinal interactions (Nikonorova et al., 2023; Taelman et al., 2022). This advancement might be crucial for evaluating the subtleties of E171's effects on gene expression and cellular behavior, which conventional 2D cultures and cancer cell lines may not adequately capture (Nikonorova et al., 2023; Taelman et al., 2022). Such a model enhances the predictive reliability in health risk assessments and aligns with the 3Rs principles (Schoonjans et al., 2023; Hubrecht and Carter, 2019).

In this study, we used human iPSC-derived colon organoids to evaluate the potential adverse effects of E171 exposure. We assessed the effects of E171 on cell viability, ROS formation, DNA damage, and changes in gene expression through RNA sequencing. We hypothesize that E171 exposure increases ROS formation, induces DNA damage, and alters the expression of inflammation- and cancer-related genes, eventually promoting CRC development.

2. Material and methods

2.1. E171 particle characterization

Sensient Technologies Company in Mexico kindly donated E171. E171 was analyzed following the NanoGenoTox protocol with spICP-MS (Thermo Scientific iCap) (Jensen et al., 2011). In short, ~15 mg of pristine E171 was dispersed in 6 mL 0.05 % BSA to reach a 2.5 mg/mL concentration, followed by probe sonication (Branson 2200, Branson Ultrasonic SA, Danbury, CT, USA) for 16 min at 4 W.

For the characterization by the spICP-MS method, samples were diluted to respect the single particle rule. Samples were analyzed for the presence of ^{48}Ti using ICP-TQ-MS operated in SQ and 1 ms dwell time. The instrument was calibrated with the ionic Ti standards (1–10 μg/L) and NanoComposix 60 nm AuNPs (60 nm). Raw data was processed using the modified "RIKILT single particle tool" to determine the size and size distribution (Verleysen et al., 2020). Only the size and size distribution were evaluated (Verleysen et al., 2020). For TEM analysis, undiluted dispersed E171 was transferred to grids (Carbon Filnus on 400 Mesh Grids Copper) using the drop-on-grid method and analyzed using a JEM-1400 TEM instrument. Whenever possible, > 60 pictures for each sample were taken, and results were processed using the "ParticleSizer" plug-in into ImageJ. This plug-in was developed within the NanoDefine project (NanoDefine, 2016). E171 was furthermore analyzed using a Malvern NanoZ devise to determine dynamic light scattering (DLS) and zeta potential. In short, all samples were diluted to a final concentration of 100 μg/mL using MQ water. DLS was set to 25 °C, incubation time 0 s, and DTS0012 or DTS1070 cuvettes were used to measure hydrodynamic diameter (HD) and zeta-potential, respectively. All samples were measured in triplicates and averaged.

2.2. Cell culture

The iPSC-derived colon organoids (#SCC300, Merck, Rahway, USA) were cultured according to the manufacturer's protocol. In short, the iPSC-derived organoids were cultured in 3dGRO™ Expansion Medium (#SCM304, Merck. Rahway, USA) supplemented with 1× PenStrep (Gibco, New York, USA) and 10 μM ROCK inhibitor (Y-27632, AbMol Bioscience, Houston, USA). The organoids were exposed to E171

ranging from 0.1 – 1000 μg/mL in 3dGRO™ Expansion Medium (1:10 dilution) from stock solutions of 0.1, 1.0, 2.5, and 10 mg/mL of E171. Therefore, in addition to the initial particle characterization, we prepared and analyzed 6 mL of stocks at 0.1, 1.0, 2.5, and 10 mg/mL of E171 following the same procedure with small deviations to the Nanogenotox dispersion protocol. Instead of probe sonication, the samples were vortexed and bath sonicated for 16 min at 37 kHz. All stock solutions were diluted at least 1:10 in the 3dGRO™ Human Colon Organoid Expansion Medium (Sigma-Aldrich) for subsequent experiments (Jensen et al., 2011). Particle size, size distribution, HD, and zeta-potential were analyzed via spICP-MS, TEM, and DLS, as described in section 2.1.

The medium was replaced daily for the first two days with the medium containing ROCK inhibitor to increase stem cell survival, proliferation, and spheroid formation. Afterward, the organoids were maintained in the medium without the ROCK inhibitor but with antibiotics. The medium was refreshed every other day. The organoids were passaged every 10–12 days to prevent over-confluency and maintain healthy growth. The passaging involved dissociating the organoids from the growth factor reduced matrigel (#CLS356231, Corning, New York, USA) through mechanical breaking up of the matrigel domes with ice-cold 1× PBS and a 3dGRO™ Organoid Dissociation Reagent (ODR, #SCM300, Merck, Rahway, USA) to remove the old matrigel, followed re-encapsulation in fresh matrigel. The split ratio at passaging was typically 1:2, adjusted based on the growth rate and density of the organoids. The iPSC-derived human colon organoids were cultured at 37 °C and 5 % CO_2. Cell passages 4–10 were used for the experiments. All following experiments were performed in biological and technical triplicates, resulting in nine sample per condition.

2.3. Cell viability

The toxicity profile was assessed by measuring cell viability via ATP levels using the 3D CellTiter-Glo assay (G9681, Promega, Madison, USA), following the manufacturer's protocol with minor adjustments. After 24-h exposure to vehicle control (VC) or E171 concentrations of 0.1, 10, 100, and 1000 μg/mL, the medium was removed, and the organoid domes were washed with 100 μL of 1× PBS. Next, the PBS was removed, 100 μL of the kit's lysis reagent was added, and the domes were homogenized to break down the matrigel and to disrupt the organoid's 3D-structure for cell lysis. To break down the domes, we placed the cell culture plates on a Scilogex MX-M 96-well plate shaker for 30 min at room temperature, set to 1000 rpm. Following 30 min of vigorous shaking, 100 μL of the homogenate was transferred to a white opaque 96-well plate (Corning, NY, USA), and luminescence was measured using a GloMax® 96 Microplate Luminometer (Promega, Madison, USA). Luminescence values, corresponding to ATP levels, were normalized to the DNA content of each well, which was determined using the same cell lysate according to the PicoGreen Assay (P7589, Invitrogen, Waltham, USA) manufacturer's protocol.

2.4. Oxidative stress and ROS generation

In this study, the detection and quantification of superoxide species in iPSC-derived 3D colon organoids exposed to E171 were carried out using Electron Spin Resonance (ESR) spectroscopy with 1-hydroxy-3-methoxycarbonyl-2,2,5,5-tetramethylpyrrolidine (CMH, NOX-02.2-100 mg, Noxygen, Elzach, Germany) as the spin probe for superoxide anions (Scheinok et al., 2018). Five organoid domes per experimental condition were selected to ensure an adequate number of cells for ESR analysis. The organoids were washed twice with 1× PBS before being treated with VC, 0.1, 10, and 1000 μg/mL of E171 concentrations in 3dGRO™ Expansion Medium for two hours.

After one hour of incubation, the culture medium was supplemented with CMH diluted in Krebs-HEPES buffer (KHB) to a final concentration of 0.5 mM CMH. After two hours of incubation, the organoids were placed on ice to stop any further metabolic activity, and the cell culture medium was carefully transferred to Eppendorf tubes for ESR spectroscopy analysis.

After removing the medium, the organoids were collected using ice-cold 1× PBS. The organoids were centrifuged at 1100 rpm for 5 min at 4 °C, after which the PBS was aspirated and replaced with 100 μL of ODR in each tube to facilitate cell dissociation. After a ten-minute incubation at room temperature with several resuspensions, the samples were centrifuged at 1500 rpm for 5 min at 4 °C. The supernatant was removed, and the single cells were resuspended in 125 μL of 1× PBS. This cell suspension was immediately subjected to ESR spectroscopy to measure the superoxide-dependent signals.

To analyze the samples, 100 μL of media or cell suspension was transferred into a 100 μL glass capillary (Brand, Eberstadt, Germany). The glass capillary was placed in the resonator of the ESR spectrometer. ESR measurements were performed on a Bruker EMX 1273 spectrometer with an ER 4119HS high-sensitivity resonator and a 12 kWE power supply operating at X band frequencies. The ESR was set to 9.68 GHz power, 50.41 mW; modulation frequency, 100 kHz; modulation amplitude, 1G; sweep time 41.94 s; time constant, 40.96 ms; sweep width, 50 G; and number of scans 10. The biological triplicates ($n = 3$) were measured in duplicate and analyzed using WinEPR software (Brueker, Bremen, Germany). Radical signals were identified in the spectrum and quantified via peak height in arbitrary units (A.U.).

2.5. DNA damage assessment

In this study, DNA damage was assessed using the standard alkaline and FPG alkaline comet assay, adapted to suit 3D cell culture models based on the protocol described by Collins et al. (Collins et al., 2023). Initially, iPSC-derived colon organoids were cultured for 12 days in a 3dGRO™ Expansion Medium, following the guidelines in section 2.2. Subsequently, E171 stock solutions were mixed with the culture medium to achieve the designated exposure concentrations outlined in section 2.1. Organoids were exposed to 10, 100, 250, and 1000 μg/mL of E171 or a VC for 24 h. After exposure, the culture medium was discarded, and the matrigel domes containing the organoids were washed once with 1× PBS.

Next, ice-cold 1× PBS was used to collect at least three domes of organoids per condition, ensuring an adequate cell number for the experiment. The collected organoids were centrifuged at 1100 rpm for 5 min at 4 °C, and the supernatant was carefully removed to discard matrigel residues. Cell dissociation was achieved by treating the cell pellet with ODR to obtain single cells and disrupt the three-dimensional structure of the organoids. The process involved adding 100 μL of ODR to the cells, pipetting up and down ten times, followed by adding another 400 μL of ODR, more pipetting, and a 10-min incubation at room temperature with continuous rocking.

After dissociation, the cell suspension was centrifuged at 1100 rpm for 5 min at 4 °C, the supernatant was discarded, and the cells were resuspended in 150–200 μL of 1× PBS. An automated cell counter (Illumina, San Diego, USA) and Trypan Blue staining were used to determine cell concentration, adjusting the cell number with 1× PBS when the concentration exceeded 1×10^6 cells/mL. A 1.5 % solution of Low Melting Point (LMP) agarose (SLBF3048V, Sigma Aldrich, Saint Louis, USA) was prepared for the comet assay. Cells were mixed with LMP agarose to a final concentration of 0.5 % LMP. A drop of 45 μL cell-LMP suspension was placed per spot on slides pre-coated with 0.75 % Normal Melting Point agarose (16500–500, Invitrogen, Waltham, USA). After covering the cells with a coverslip and allowing the mixture to solidify at 4 °C for 45 min, the coverslips were removed, and the cells were lysed overnight at 4 °C in lysis buffer containing 2.5 M NaCl, 100 mM EDTA, 10 mM Tris, 240 mM NaOH, 1 % Triton-X, and 10 % DMSO.

Following lysis, the slides underwent two washing steps with 1× Buffer B and were placed on an ice-cold metal plate to maintain low temperatures and avoid premature enzyme activation. The slides were exposed to either 50 μL of 1:3000 diluted FPG enzyme (M02405, New

England Biolabs, Ipswich, USA) in Buffer B or 50 μL Buffer B (standard alkaline comet assay) alone for 30 min at 37 °C. Following the incubation, the slides were immediately submerged in electrophoresis buffer (300 mM NaOH, 1 mM EDTA, pH > 12) for unwinding, incubating them at 4 °C for 20 min. Electrophoresis was performed for 20 min at 200 V. After electrophoresis, the slides were washed twice in 1× PBS and dehydrated in 70 % ethanol for 30 s before being left to dry for 2–3 days in preparation for imaging.

To visualize and quantify DNA damage, the slides were stained with 3× gel red for 20 min and analyzed using COMET IV software. At least 100 cells per condition were analyzed across three biological replicates ($n = 3$). To ensure accuracy, all slides were independently scored a second time by a blinded operator.

2.6. RNA isolation

Following 24 h of incubation to 10, 100, 250, and 1000 μg/mL of E171 or VC, the medium was removed from the plates, and 100 μL of ice-cold 1× PBS was added into each well to collect the organoids into a 1.5 mL Eppendorf tube. The organoids were centrifuged at 1100 rpm for 5 min at 4 °C, and the supernatant containing the excess matrigel was removed. Next, a total volume of 700 μL of QIAzol Lysis reagent (Qiagen, Venlo, The Netherlands) was added to each tube. Complete homogenization of organoids in the lysis reagent was reached by vigorous pipetting and vortexing for 1 min. Samples were immediately frozen at −80 °C until further processing. RNA isolation was performed using the miRNeasy Mini Kit (Qiagen, Venlo, The Netherlands), following the manufacturer's protocol for animal cells, which included a DNase treatment. Total RNA yield was measured on Qubit according to the manufacturer's protocol (Thermo Fisher Scientific, Waltham, Massachusetts, USA), and RNA quality was assessed using RNA Pico-/Nanochips on a 2100 Bioanalyzer (Agilent Technologies, Leuven, Belgium). All samples with an RNA integrity number (RIN) > 7 and a total amount of RNA ≥ 100 ng were used for RNA sequencing. We prepared three technical and three biological (cell passage 6–8) replicates per concentration, totaling nine replicates per condition.

2.7. Library preparations and RNA bulk sequencing

Samples containing purified RNA were prepared for sequencing using a NEX Poly(A) Beads 2.0 auto kit (Revvity, Groningen, The Netherlands) on a Zephyr G3 NGS workstation (CLS150362, Revvity, Groningen, The Netherlands). After library preparation, the samples were sequenced on an S1 flow cell (Illumina, San Diego, USA) on the NovaSeq 6000 system (Illumina, San Diego, USA) using the NEX Rapid Dir RNAseq auto kit 2.0 (Revvity, Groningen, The Netherlands).

2.8. Pre-processing and data analysis

Raw RNA sequencing data were obtained as BCL files and converted to fastq files using BCL2FastQ (v2.20.0.422). The fastq files were processed using the R-ODAF pipeline (Verheijen et al., 2022). In short, reads were trimmed with fastp (v0.20.0) with a head crop of 12 bases. MultiQC (v1.7) quality control after trimming indicated good sequencing quality (all bases > Q35) with a sequencing depth between 41.7 M and 66.2 M per sample. These reads were mapped to the genome (GRCh38_112) with STAR (v2.7.9a) and quantified using RSEM (v1.3.1). The resulting raw counts were processed using DESeq2 (v1.40.2). Multiple filters were applied to guarantee reliable differentially expressed genes. Genes were kept for differential expression analysis if sequencing depth was >5 M and the gene was expressed (> 1 CPM) in at least 75 % of samples belonging to one of the groups. After the statistical analysis, results were filtered according to R-ODAF recommendations to exclude spurious spikes and ensure biological relevance (median of one group larger than the third quantile of the other) (Verheijen et al., 2022). Genes with an FDR < 0.05 were considered statistically significant differentially expressed genes (DEGs).

2.8.1. Pathway analysis and GSEA analysis

The web-based interface Multi Ontology Enrichment Tool (MOET) (Vedi et al., 2022) was used to identify enriched pathways among the DEGs for the E171 concentrations. The analysis was run with default settings and species set to "Human," ontology set to "Pathway," and symbols set to "Ensembl Gene". Pathways with a p-value <0.05 were considered significantly enriched. Additionally, we performed a gene set enrichment analysis (GSEA) using the "stat" value obtained from the DESeq2 analysis for gene ranking. The stat value is based on t-statistics accounting for effect size (log2foldchange) and set size (standard error). Enriched gene sets and their respective pathways were determined with ClusterProfiler using the KEGG database (Yu et al., 2012; Wu et al., 2021). A q-value <0.05 (Bonferroni) was set to determine significantly enriched pathways.

2.8.2. Statistical analysis

The data from the cell viability, oxidative stress, and DNA damage assays were analyzed by GraphPad Prism 10. The data was first checked for statistical outliers by ROUT, multiple outlier testing with Q = 1 %. Outliers were removed, and data was checked for normality by the Shapiro-Wilk normality test for groups of <60 data entries and the Kolmogorov-Smirnov normality test for groups of >60. A one-way ANOVA was applied when all groups were normally distributed, with Bonferroni <0.05. A nonparametric test with Dunn's < 0.05 was applied if one or more groups were not normally distributed. Data was displayed as mean and standard deviation (SD) for parametric distribution and median and 95 % confidence interval (CI) for nonparametric distribution.

3. Results

3.1. E171 particle characterization

E171 was characterized via spICP-MS, TEM, and DLS following the NanoGenoTox dispersion protocol's dispersion and subsequent dispersion in 3dGRO™ Expansion Medium. The initial characterization showed that the E171 median particle size was 78 nm via spICP-MS and 79 nm via TEM measurement (Fig. 1) (Bischoff et al., 2020). The median percentage of particles <100 nm was 73 % and 75 %, respectively (Table 1). DLS measurements showed a mean HD of 353 nm (PDI = 0.19) and a zeta potential of −31.4 mV. The characterization in 3dGRO™ Expansion Medium at 10, 100, 250, and 1000 μg/mL showed a median particle size of 256, 220, 225, and 221 nm, respectively. The dispersions showed a nanoparticle fraction of 4, 13, 16, and 12 % for the concentrations of 10, 100, 250, and 1000 μg/mL of E171. While the E171 particles showed a relatively stable aggregate size between 220 and 256 nm when analyzed with spICP-MS, the same dispersions showed a difference in their aggregation size when analyzed via DLS. While the concentrations ranging from 10 to 250 μg/mL showed a similar HD of 351–396 nm, we observed an increased mean HD of 637 nm at the 1000 mg/mL stock, with a simultaneous decrease in zeta-potential to −25.2 mV.

3.2. Cell viability

The assessment of cell viability in colon organoids was based on quantifying ATP release, followed by normalization to DNA concentration of each experimental condition. Fig. 2 A shows the state of the organoids following 12 days of culturing, highlighting the differences in their state of differentiation and the need for normalization. Following 24 h of exposure, none of the E171 concentrations affected cell viability (Fig. 2 B).

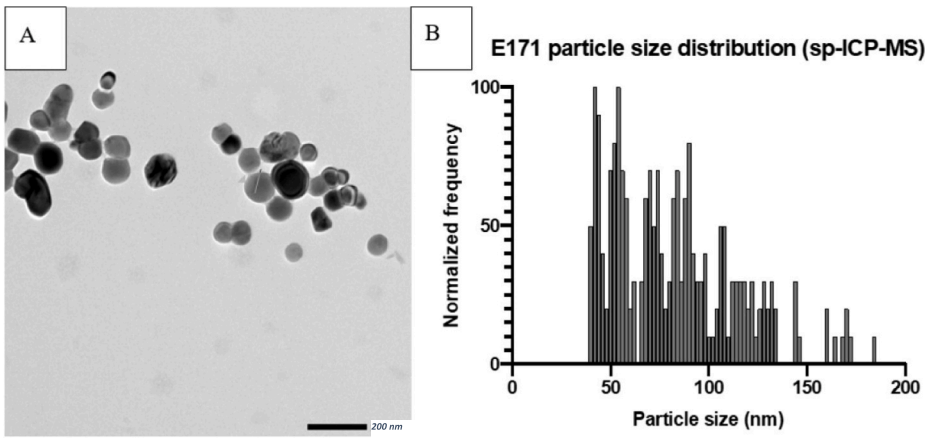

Fig. 1. Fig. 1A shows a exemplary TEM image of E171 particles. Fig. 1B shows a histogram size distribution of E171 particles as measured via spICP-MS.

Table 1
Physicochemical characterization of pristine E171 according to the NanoGenoTox dispersion protocol in 0.05 % BSA and exposure concentrations of E171 in 3dGRO™ Expansion Medium for organoid cell culture.

E171 dilutions	spICP-MS (median, nm)	spICP-MS (median % < 100 nm)	TEM (median, nm)	TEM (median, % < 100 nm)	HD (mean, nm)	PDI (mean)	Zeta potential (mean, mV)	pH (mean)
pristine	76	73	79	75	353	0.19	−31.4	7.0
10 µg/mL in medium	256	4	N/A	N/A	375	0.14	−14.5	7.0
100 µg/mL in medium	220	13	N/A	N/A	396	0.18	−10.2	7.1
250 µg/mL in medium	225	16	N/A	N/A	351	0.13	−15.7	7.0
1000 µg/mL in medium	221	12	N/A	N/A	637	0.19	−25.3	7.1

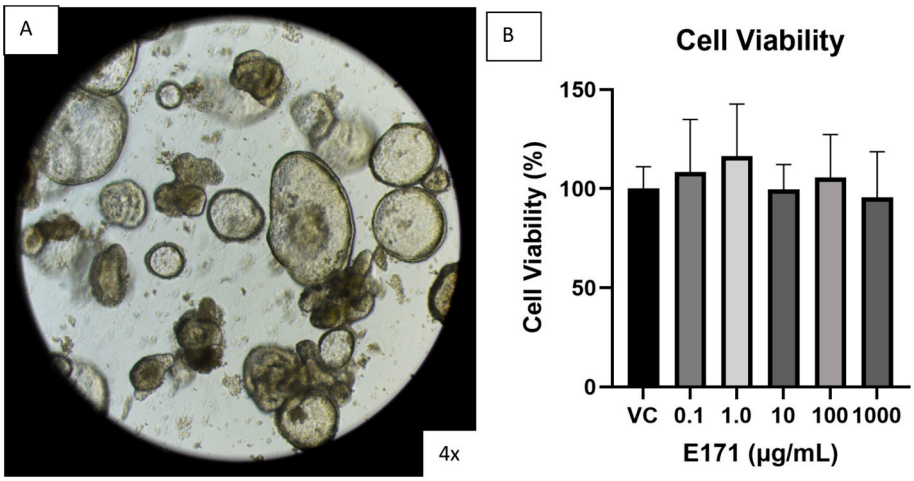

Fig. 2. A) Shows an exemplary light microscopy image of the iPSC-derived colon organoids after 12 days of cell culture differentiation, right before the exposure to E171 for 24 h at 4× B) Human iPSC-derived colon organoids did not show any effect of reduced cell viability, following 24 h of exposure to E171. Fig. 2 A shows cell viability of organoids in percentage, normalized to DNA concentration per condition, displayed as mean and SD.

3.3. Oxidative stress and ROS generation

ROS levels were measured using ESR spectroscopy to assess oxidative stress. Utilizing the spin-probe CMH, we identified and quantified superoxide radicals following exposure to E171 for two hours. We measured a statistically significant increase in superoxide radicals at 1000 µg/mL of E171, compared to the VC (Fig. 3 A). E171 possesses an innate mechanism to produce ROS (Bischoff et al., 2024). The lower concentrations, 0.1 and 10 µg/mL, slightly increased ROS levels by a factor of 1.2 and 1.4, respectively. Fig. 3 B shows that the cell culture medium containing E171 particles did not increase ROS when measured without the presence of colon organoids, demonstrating that the ROS were only generated in the presence of cells and E171 (Fig. 3 B).

3.4. Alkaline comet assay

To determine DNA damage, we performed a standard alkaline comet assay and an FPG alkaline comet assay. In alkaline conditions, E171 significantly induced DNA damage at 100, 250, and 1000 µg/mL following 24 h of E171 exposure (Fig. 4 A). VC samples showed an average of 6.4 % DNA damage, while the exposure conditions increased DNA damage to 11.0 %, 15.2 %, and 21.5 %, at 100, 250, and 1000 µg/mL, respectively. Exemplary images made with the COMET IV software, per conditions were added to the Supplementary data (*Supplementary data*).

As the FPG enzyme converts the oxidative base modification 8-Oxo-Guanine to DNA single-strand breaks, the FPG alkaline comet assay is

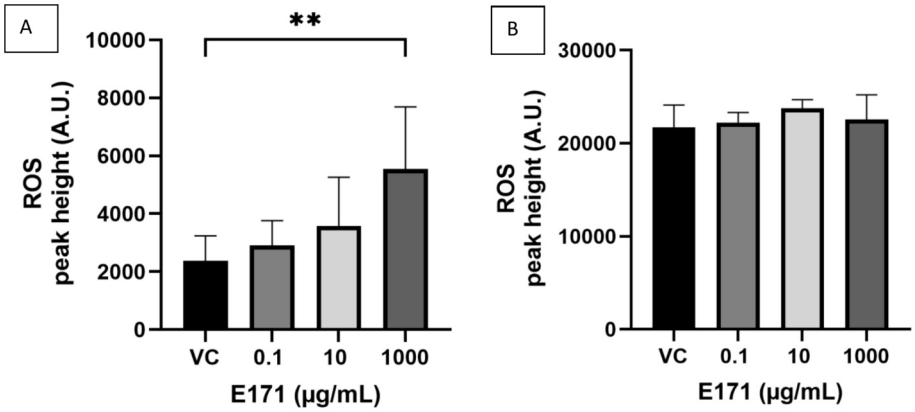

Fig. 3. A) Shows the concentration of superoxide radicals in arbitrary units (A.U.), indicating the level of oxidative stress, which is increasing with increasing E171 concentration. B) Shows the ROS levels in cell culture medium, containing E171. The analysis showed no differences in ROS levels between VC and exposure conditions. Graphs display mean and SD. Statistical significance was assessed with One-Way-ANOVA and Bonferroni correction of <0.05, ** < 0.01).

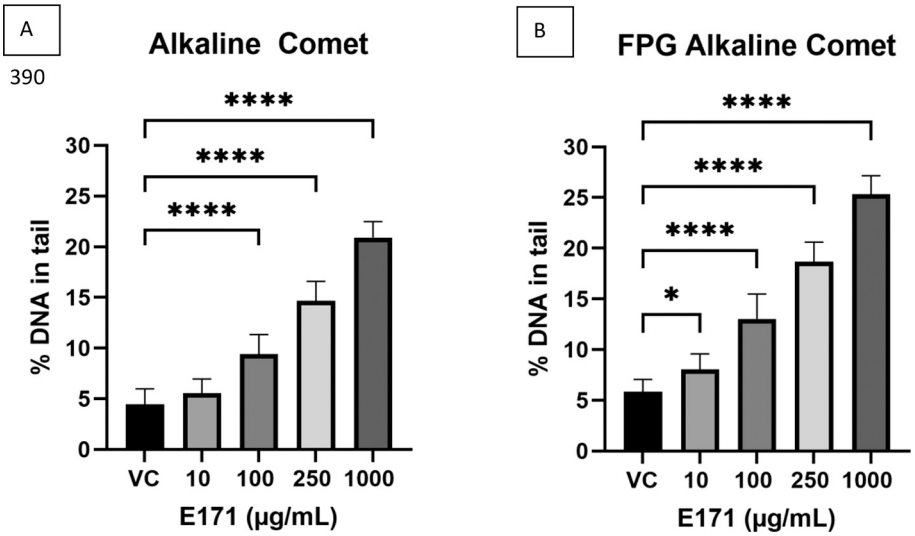

Fig. 4. Fig. A) and B) display the results of the standard alkaline and FPG alkaline comet assay, respectively. Exposure to E171 resulted in a dose dependent increase of DNA damage. Data is displayed as median and 95 % CI. Statistical significance was assessed via One-Way ANOVA with Bonferroni correction <0.05, * < 0.05, **** < 0.0001.

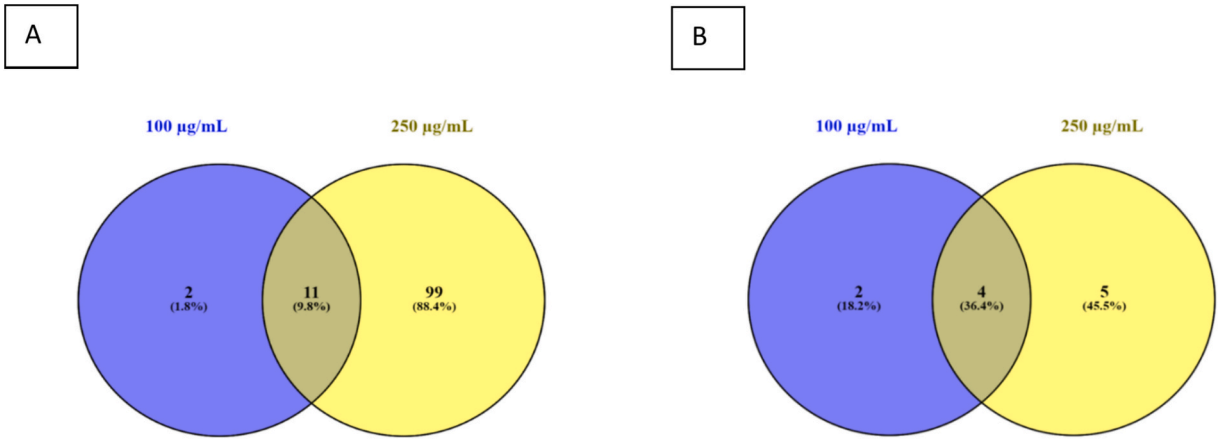

Fig. 5. A) Venn Diagram shows the overlap of DEGs (FDR < 0.05). Out of 13 DEGs identified at 100 µg/mL, 11 DEGs were also found at 250 µg/mL. B) Shows the overlap in enriched pathways between 100 and 250 µg/mL of E171. No DEGs, and subsequently no pathways were identified for 10, and 1000 µg/mL of E171 exposure.

more sensitive in detecting DNA damage compared to the standard alkaline comet assay. All exposure conditions significantly increased DNA damage following 24 h of E171 exposure (Fig. 4 B). The VC showed an average of 7.8 % DNA damage, while DNA damage in the exposure conditions 10, 100, 250, and 1000 μg/mL of E171 increased to 9.9 %, 14.2 %, 19.2 %, and 25.7 %, respectively.

3.5. RNA sequencing, pathway analysis, and GSEA

RNA isolation of colon organoid samples yielded an average of 50.4 ng/μL of RNA, with an average RIN value of 8.5. Following sequencing, data-clean-up, and pre-processing via the standardized R-ODAF pipeline, we identified DEGs using DESeq2 (Verheijen et al., 2022). DEG analysis (FDR <0.05) resulted in 13 and 110 DEGs following the exposure to 100 and 250 μg/mL of E171, respectively. No DEGs were detected for 10 and 1000 μg/mL of E171 exposure for 24 h. Fig. 5 A) and B) show the overlap of identified DEGs and pathways between 100 and 250 μg/mL of E171 exposure, respectively.

Fig. 5 A shows that out of 13 DEGs identified at 100 μg/mL, most (11 DEGs) were also found in the higher dose of 250 μg/mL of E171. These 11 genes were SIPA1L3, RPL34, RPS6, RPS8, RPL10, EEF1A1, RPL29, RPL9, BCL2L15, EEF1A1P5, and RPL39. All shared DEGs showed the same directionality, with SIPA1L3 being suppressed, while all other DEGs were activated. Furthermore, four enriched pathways were shared between the two exposure concentrations. Namely, “translational pathway”, “ribosome biogenesis pathway”, “translation elongation pathway”, and “pathway pertinent to DNA replication and repair cell cycle maintenance of genomic integrity of RNA and protein biosynthesis”. The overlap indicates common genetic alterations related to ribosomal and translation activity, as well as DNA replication and repair. Additional pathways were identified at 250 μg/mL, which showed effects on chaperon-mediated autophagy pathways, G-Protein Coupled Receptor signaling (Arf, Ras family), and altered Notch signaling (Table 2).

GSEA also showed the most potent transcriptional response at 250 μg/mL of E171, with 68 pathways being activated or suppressed. The dose groups of 10 and 100 μg/mL of E171 showed a milder response, with a total of 15 pathways affected. At the same time, 1000 μg/mL of E171 showed the modulation of 37 pathways. Fig. 6 shows an overview of the suppressed and activated pathways.

GSEA revealed activated pathways related to the ribosome, Coronavirus disease, and diabetic cardiomyopathy for 100, 250, and 1000 μg/mL of E171. Most activated pathways were shared between 250 and 1000 μg/mL of E171, namely metabolic pathways, non-alcoholic fatty liver disease, oxidative phosphorylation, thermogenesis, chemical carcinogenesis – reactive oxygen species, peroxisome, Parkinson’s disease, PPAR signaling pathway, carbon metabolism, and glycolysis/gluconeogenesis—notably, many pathways related to the cell’s metabolic activity and its response to oxidative stress. Unique pathways related to cellular metabolism occurred at 250 μg/mL of E171 with drug metabolism – cytochrome P450, amino sugar and nucleotide sugar metabolism, drug metabolism, other enzymes, and metabolism of xenobiotics by cytochrome P450, as well as the citric cycle (TCA cycle) for 1000 μg/mL of E171 (Fig. 6).

Exposure to 10 and 100 μg/mL of E171 showed suppression of 8 pathways related to genetic information processing (“translation”, “folding, sorting, degradation”), organismal systems (“immune system”), metabolism (“glycan biosynthesis and metabolism”), human disease (“infectious disease”), environmental processing (“signaling transduction”), and cellular processes (“transport and catabolism”).

Table 2
Enriched pathways identified from DEG lists (FDR < 0.05) of 100 and 250 μg/mL of E171 for 24 h.

E171 (μg/mL)	Category	Pathway	Gene Count	Genes	p-value	q-value
100	Translation	translation pathway	10	EEF1A1, RPL10, RPL29, RPL34, RPL39, RPL9, RPS19, RPS27, RPS6, RPS8	6.09E-15	1.10E-13
100	Translation	ribosome biogenesis pathway	9	RPL10, RPL29, RPL34, RPL39, RPL9, RPS19, RPS27, RPS6, RPS8	2.51E-13	4.52E-12
100	DNA/RNA damage	pathway pertinent to DNA replication and repair cell cycle maintenance of genomic integrity RNA and protein biosynthesis	10	EEF1A1, RPL10, RPL29, RPL34, RPL39, RPL9, RPS19, RPS27, RPS6, RPS8	2.41E-06	4.34E-05
100	Translation	translation elongation pathway	1	EEF1A1	5.03E-03	9.05E-02
100	Translation	regulatory pathway	10	EEF1A1, RPL10, RPL29, RPL34, RPL39, RPL9, RPS19, RPS27, RPS6, RPS8	6.48E-03	1.17E-01
100	Translation	chaperone-mediated autophagy pathway	1	EEF1A1	2.00E-02	3.60E-01
250	Translation	ribosome biogenesis pathway	18	RPL10, RPl12, RPL15, RPL18, RPL29, RPL34, RPL35A, RPL36A, RPL37, RPL39, RPL9, RPLP0, RPS14, RPS18, RPS3A, RPS4X, RPS6, RPS8	3.20E-15	7.30E-13
250	Translation	translation pathway	19	EEF1A1, RPL10, RPl12, RPL15, RPL18, RPL29, RPL34, RPL35A, RPL36A, RPL37, RPL39, RPL9, RPLP0, RPS14, RPS18, RPS3A, RPS4X, RPS6, RPS8	7.07E-15	1.61E-12
250	DNA/RNA damage	pathway pertinent to DNA replication and repair cell cycle maintenance of genomic integrity RNA and protein biosynthesis	24	DHX16, EEF1A1, H3-3A, H3—3B, LAMTOR5, RPL10, RPl12, RPL15, RPL18, RPL29, RPL34, RPL35A, RPL36A, RPL37, RPL39, RPL9, RPLP0, RPS14, RPS18, RPS3A, RPS4X, RPS6, RPS8, SYK	1.52E-03	3.47E-01
250	Signal Transduction	Arf family-mediated signaling pathway	2	AP2A1, GIT1	1.31E-02	1.00E+00
250	Human disease: cardiovascular	myocardial infarction pathway	1	LGALS2	2.50E-02	1.00E+00
250	Translation	translation elongation pathway	1	EED1A1	2.50E-02	1.00E+00
250	Signal Transduction	Ras superfamily-mediated signaling pathway	3	AP2A1, ARPC3, GIT1	2.73E-02	1.00E+00
250	Metabolism	paracetamol pharmacokinetics pathway	2	ABCC1, UGT1A6	3.09E-02	1.00E+00
250	Signal Transduction	altered Notch signaling pathway involving the main players	1	JAG1	3.32E-02	1.00E+00

Fig. 6. GSEA results of activated and suppressed pathways, following E171 exposure for 24 h, in 3D colon organoids in comparison to the vehicle control groups. GeneCount indicates the number of genes enriched in a specific gene set, while the color indicates the significance of the q-value.

Most suppressed pathways were reported for 250 and 1000 µg/mL of E171. These included extracellular matrix (ECM) -receptor interaction, signaling pathways regulating pluripotency of stem cells, human papillomavirus infection, Hippo signaling pathway, PI3K-Akt signaling pathway, pathways in cancer, focal adhesion, thyroid hormone signaling pathway, Wnt signaling pathway, efferocytosis, regulation of actin cytoskeleton, PD-L1 expression and PD-1 checkpoint in cancer, as well as EGFR tyrosine kinase inhibitor resistance (Fig. 6). A detailed overview of all pathways per dose group, with their set size, enrichment score, and normalized enrichment score (NES), can be found in Table 3. *Supplementary Table 1–5* details the identified genes and visual overviews of NES scores per dose group.

When comparing the results from the differential gene expression analysis with the GSEA, we observed a dose response fitting the ROS measurements and comet assay results, which indicated a similar response of the 250 and 1000 µg/mL of E171 dose groups. Both transcriptional analysis approaches showed pathways affected that relate to ribosome biogenesis in eukaryotes and general ribosomal activity, which are responsible for the assembly of the ribosomal components, protein translation, and biosynthesis. Furthermore, pathways such as Arf-mediated signaling pathways and Ras superfamily-mediated signaling pathways suggest the modulation of signaling cascades that interact with the PI3K-Akt pathway, which is crucial for cell growth, survival, and metabolism. Additionally, pathways pertinent to DNA replication and repair, cell cycle maintenance, and genomic integrity might overlap with the hippo pathway signaling detected via GSEA, which controls cell proliferation and apoptosis. Other functional overlaps include DNA replication, repair and genomic integrity, oxidative stress, cell cycle, translation, protein synthesis, autophagy, cellular homeostasis, signaling pathways (MAPK, Wnt, PI3K), and metabolic pathways. Gene co expression networks for the concentrations of 10, 100,250, and 1000 µg/mL are displayed in the Supplementary materials.

In summary, DEGs indicated a moderate transcriptional response to 24 h of E171 exposure, with only 100 and 250 µg/mL of E171 showing DEGs, which revealed modulation of pathways related to ribosome, translation, DNA damage/repair, and signal transduction. GSEA uncovered a more consistent dose response to E171 exposure. However, a slight decrease in transcriptional response at 1000 µg/mL of E171 was still observed, potentially related to the increased aggregation of E171 particles at 1000 µg/mL and consequently lower bioavailability.

4. Discussion

In this study, we used human iPSC-derived colon organoids to investigate the potential adverse effects of E171 exposure. Our results demonstrate that E171 did not impact cell viability. However, it induced ROS generation, caused DNA damage, and altered gene expression profiles in a dose-dependent manner. The RNA sequencing data revealed DEGs related to a metabolic shift toward carbon metabolism, inflammation, ECM modulation, signal transduction, and cancer-related pathways. These findings provide novel insights into the potential molecular mechanisms underlying E171-induced toxicity in human colon cells.

We investigated the potential cytotoxicity of E171 without measuring any decrease in cell viability following a 24-h exposure to E171 for any of the administered concentrations. This corroborates

Table 3
Results of the GSEA, including the dose of E171, the enriched KEGG pathway, enrichment scores, and normalized enrichment scores (NES), as well as significance levels.

Dose E171 (μg/mL)	Description	Enrichment Score	NES	p-value	q-value
10	Ribosome biogenesis in eukaryotes	−0.52407	−2.22	5.31E-07	1.64E-04
10	Nucleocytoplasmic transport	−0.43003	−1.91	7.23E-05	1.12E-02
10	Leukocyte transendothelial migration	0.424184	1.88	1.15E-04	1.18E-02
10	NOD-like receptor signaling pathway	0.365596	1.78	1.73E-04	1.34E-02
10	Protein processing in endoplasmic reticulum	−0.35883	−1.70	2.63E-04	1.63E-02
10	Mannose type O-glycan biosynthesis	−0.62626	−1.92	7.17E-04	3.30E-02
10	Proteasome	−0.50592	−1.89	7.46E-04	3.30E-02
10	Pertussis	0.454163	1.86	1.13E-03	3.98E-02
10	NF-kappa B signaling pathway	0.389582	1.74	1.16E-03	3.98E-02
100	Ribosome	0.840975	3.98	1.00E-10	1.62E-08
100	Coronavirus disease - COVID-19	0.714718	3.54	1.00E-10	1.62E-08
100	Lysosome	−0.44759	−1.90	6.95E-06	7.51E-04
100	Glycosaminoglycan biosynthesis - heparan sulfate / heparin	−0.75681	−2.15	1.11E-05	8.96E-04
100	Bile secretion	−0.53792	−1.98	9.70E-05	6.29E-03
100	Diabetic cardiomyopathy	0.324875	1.60	3.07E-04	1.66E-02
100	Mannose type O-glycan biosynthesis	−0.64486	−1.89	8.36E-04	3.87E-02
250	Ribosome	0.834145	3.89	1.00E-10	6.00E-09
250	Coronavirus disease - COVID-19	0.685964	3.35	1.00E-10	6.00E-09
250	Oxidative phosphorylation	0.572592	2.63	1.00E-10	6.00E-09
250	Parkinson's disease	0.447088	2.27	1.00E-10	6.00E-09
250	Non-alcoholic fatty liver disease	0.477351	2.24	4.83E-10	2.32E-08
250	Chemical carcinogenesis - reactive oxygen species	0.430843	2.13	6.32E-10	2.53E-08
250	Diabetic cardiomyopathy	0.442825	2.16	9.52E-10	3.26E-08
250	Prion disease	0.410062	2.08	1.30E-09	3.89E-08
250	Huntington disease	0.364058	1.87	7.06E-08	1.88E-06
250	Thermogenesis	0.396497	1.95	7.91E-08	1.90E-06
250	Peroxisome	0.536673	2.29	2.92E-07	6.37E-06
250	Metabolic pathways	0.239509	1.40	4.00E-07	7.99E-06
250	Amyotrophic lateral sclerosis	0.337965	1.77	5.92E-07	1.09E-05
250	ECM-receptor interaction	−0.6345	−2.27	1.38E-06	2.37E-05
250	Hippo signaling pathway	−0.46515	−1.98	3.47E-06	5.56E-05
250	Human papillomavirus infection	−0.37278	−1.73	8.00E-06	1.20E-04
250	MAPK signaling pathway	−0.37765	−1.73	2.85E-05	4.03E-04
250	Pathways of neurodegeneration - multiple diseases	0.292054	1.56	3.32E-05	4.31E-04
250	Pathways in cancer	−0.32	−1.54	3.41E-05	4.31E-04
250	MicroRNAs in cancer	−0.41012	−1.78	3.74E-05	4.48E-04
250	Phospholipase D signaling pathway	−0.44469	−1.84	4.49E-05	5.13E-04
250	Thyroid hormone signaling pathway	−0.44679	−1.85	5.78E-05	6.30E-04
250	Signaling pathways regulating pluripotency of stem cells	−0.45531	−1.85	7.36E-05	7.68E-04
250	Focal adhesion	−0.40831	−1.77	8.86E-05	8.86E-04
250	Alzheimer's disease	0.296006	1.56	9.73E-05	9.34E-04
250	Fc gamma R-mediated phagocytosis	−0.47158	−1.88	1.17E-04	1.00E-03
250	Breast cancer	−0.45161	−1.86	1.16E-04	1.00E-03
250	Wnt signaling pathway	−0.42257	−1.80	1.11E-04	1.00E-03
250	Cytoskeleton in muscle cells	−0.41513	−1.77	1.95E-04	1.57E-03
250	Regulation of actin cytoskeleton	−0.38187	−1.69	1.96E-04	1.57E-03
250	Chronic myeloid leukemia	−0.45791	−1.80	2.48E-04	1.92E-03
250	Axon guidance	−0.39833	−1.73	2.69E-04	2.02E-03
250	Hippo signaling pathway - multiple species	−0.61578	−1.92	3.10E-04	2.26E-03
250	Proteoglycans in cancer	−0.38424	−1.67	3.81E-04	2.69E-03
250	PI3K-Akt signaling pathway	−0.34605	−1.59	4.22E-04	2.90E-03
250	Drug metabolism - cytochrome P450	0.509604	1.91	5.25E-04	3.50E-03
250	Acute myeloid leukemia	−0.50701	−1.88	6.00E-04	3.89E-03
250	Phosphatidylinositol signaling system	−0.42666	−1.73	6.47E-04	4.09E-03
250	Amino sugar and nucleotide sugar metabolism	0.484518	1.82	9.20E-04	5.54E-03
250	PPAR signaling pathway	0.450518	1.79	9.23E-04	5.54E-03
250	Retrograde endocannabinoid signaling	0.391478	1.73	9.52E-04	5.58E-03
250	Mannose type O-glycan biosynthesis	−0.6424	−1.87	1.18E-03	6.57E-03
250	Hepatitis B	−0.37615	−1.63	1.15E-03	6.57E-03
250	Various types of N-glycan biosynthesis	0.484234	1.78	1.54E-03	8.40E-03
250	Chemical carcinogenesis - DNA adducts	0.466892	1.75	1.58E-03	8.44E-03
250	Protein export	0.535781	1.91	1.80E-03	9.40E-03
250	Polycomb repressive complex	−0.42145	−1.69	2.08E-03	1.06E-02
250	Drug metabolism - other enzymes	0.423112	1.69	2.37E-03	1.19E-02
250	Endocrine resistance	−0.41581	−1.67	2.63E-03	1.29E-02
250	Efferocytosis	−0.3667	−1.57	2.71E-03	1.30E-02
250	Biosynthesis of nucleotide sugars	0.506065	1.84	2.94E-03	1.39E-02

(continued on next page)

Table 3 (*continued*)

Dose E171 (μg/mL)	Description	Enrichment Score	NES	p-value	q-value
250	Hepatocellular carcinoma	−0.36098	−1.56	3.01E-03	1.39E-02
250	Fc epsilon RI signaling pathway	−0.47209	−1.72	3.64E-03	1.65E-02
250	Gastric cancer	−0.37791	−1.57	4.00E-03	1.78E-02
250	Rap1 signaling pathway	−0.34424	−1.49	4.57E-03	1.99E-02
250	Hedgehog signaling pathway	−0.48692	−1.74	5.20E-03	2.19E-02
250	Inositol phosphate metabolism	−0.41487	−1.61	5.16E-03	2.19E-02
250	Yersinia infection	−0.35821	−1.52	5.30E-03	2.19E-02
250	Metabolism of xenobiotics by cytochrome P450	0.425463	1.63	5.50E-03	2.20E-02
250	PD-L1 expression and PD-1 checkpoint pathway in cancer	−0.41047	−1.61	5.50E-03	2.20E-02
250	Basal cell carcinoma	−0.50525	−1.73	5.70E-03	2.24E-02
250	Th1 and Th2 cell differentiation	−0.43462	−1.63	5.98E-03	2.31E-02
250	Virion - Herpesvirus	−0.79483	−1.67	7.73E-03	2.89E-02
250	Glycolysis / Gluconeogenesis	0.419386	1.63	7.83E-03	2.89E-02
250	Carbon metabolism	0.336687	1.53	7.60E-03	2.89E-02
250	Other types of O-glycan biosynthesis	−0.49332	−1.69	8.14E-03	2.92E-02
250	Endometrial cancer	−0.4265	−1.59	8.13E-03	2.92E-02
250	Growth hormone synthesis, secretion and action	−0.38267	−1.56	8.68E-03	3.07E-02
1000	Ribosome	0.562593	2.71	1.00E-10	2.62E-08
1000	Metabolic pathways	0.254002	1.53	6.86E-10	8.99E-08
1000	Coronavirus disease - COVID-19	0.416439	2.11	7.40E-09	6.47E-07
1000	Signaling pathways regulating pluripotency of stem cells	−0.52112	−2.20	1.52E-07	9.97E-06
1000	ECM-receptor interaction	−0.63789	−2.33	2.15E-07	1.13E-05
1000	Non-alcoholic fatty liver disease	0.403532	1.95	2.68E-06	1.17E-04
1000	Oxidative phosphorylation	0.404908	1.92	7.96E-06	2.98E-04
1000	Carbon metabolism	0.417505	1.92	2.70E-05	7.84E-04
1000	PI3K-Akt signaling pathway	−0.36114	−1.71	2.54E-05	7.84E-04
1000	Human papillomavirus infection	−0.35098	−1.69	2.99E-05	7.84E-04
1000	Thermogenesis	0.323054	1.65	6.55E-05	1.56E-03
1000	Hippo signaling pathway	−0.40778	−1.80	1.08E-04	2.35E-03
1000	Diabetic cardiomyopathy	0.332706	1.66	1.34E-04	2.65E-03
1000	Chemical carcinogenesis - reactive oxygen species	0.32471	1.66	1.41E-04	2.65E-03
1000	Glycolysis / Gluconeogenesis	0.473934	1.89	1.79E-04	3.13E-03
1000	Peroxisome	0.431592	1.87	2.17E-04	3.55E-03
1000	Pathways in cancer	−0.29999	−1.51	3.45E-04	5.33E-03

Table 3 (*continued*)

Dose E171 (μg/mL)	Description	Enrichment Score	NES	p-value	q-value
1000	Efferocytosis	−0.38661	−1.71	4.95E-04	7.21E-03
1000	Nicotinate and nicotinamide metabolism	0.561887	1.93	5.98E-04	8.26E-03
1000	PD-L1 expression and PD-1 checkpoint pathway in cancer	−0.43527	−1.77	8.60E-04	1.13E-02
1000	Focal adhesion	−0.35897	−1.61	9.47E-04	1.18E-02
1000	Thyroid hormone signaling pathway	−0.39833	−1.70	1.12E-03	1.27E-02
1000	Salmonella infection	−0.31842	−1.51	1.10E-03	1.27E-02
1000	Fructose and mannose metabolism	0.526647	1.90	1.21E-03	1.32E-02
1000	Glyoxylate and dicarboxylate metabolism	0.543625	1.86	1.41E-03	1.48E-02
1000	PPAR signaling pathway	0.428051	1.74	1.67E-03	1.63E-02
1000	Parkinson's disease	0.278374	1.45	1.63E-03	1.63E-02
1000	Th17 cell differentiation	−0.44231	−1.76	1.74E-03	1.63E-02
1000	Ras signaling pathway	−0.33622	−1.52	1.92E-03	1.73E-02
1000	Citrate cycle (TCA cycle)	0.512651	1.82	2.12E-03	1.85E-02
1000	Wnt signaling pathway	−0.3646	−1.60	2.28E-03	1.93E-02
1000	Regulation of actin cytoskeleton	−0.34121	−1.55	2.45E-03	2.01E-02
1000	Growth hormone synthesis, secretion and action	−0.3891	−1.65	2.63E-03	2.09E-02
1000	TGF-beta signaling pathway	−0.39364	−1.63	2.83E-03	2.18E-02
1000	Caffeine metabolism	0.939017	1.63	3.02E-03	2.26E-02
1000	EGFR tyrosine kinase inhibitor resistance	−0.42401	−1.69	4.11E-03	2.99E-02
1000	Hedgehog signaling pathway	−0.46209	−1.68	4.94E-03	3.50E-02

other findings, as E171-induced cytotoxicity has rarely been reported in in vitro models (David et al., 2022; Kampfer et al., 2021; Bettencourt et al., 2020).

We furthermore measured superoxide radical formation following a 2-h exposure to E171. Our results showed a dose-dependent increase in superoxide levels, demonstrating the potential of E171 to induce ROS in vitro. Our findings are consistent with other studies, which showed E171-related ROS formation in various in vitro models using the DCFH-DA, GSH/GSSG ratio, and other assays for oxidative stress (Bettencourt et al., 2020; Dorier et al., 2019; Botelho et al., 2014; Vigneshwaran et al., 2021; Guo et al., 2017; Li et al., 2014; Dvoranova et al., 2014). Most importantly, the formation of ROS only occurred when E171 was in the presence of the colon organoids. No ROS formation was detected in dispersed E171 in the cell culture medium alone. This strongly suggests an interaction of E171 with the colon cells, leading to the formation of ROS.

Statistically significant increases in the levels of DNA damage were observed in the standard alkaline comet and FPG-modified alkaline comet assays. DNA damage was detected in a dose-dependent manner in both comet assay setups, highlighting the genotoxic potential of E171 in vitro. The increased DNA damage detected in the FPG comet assay indicates the presence of the oxidative base modification 8-oxo-guanine, which forms as a consequence of the increased oxidative stress and free radical interaction with the DNA. Many other studies have shown

similar results, indicating that E171 can produce DNA lesions and chromosomal aberrations (Vieira et al., 2022; Ferrante et al., 2023; Proquin et al., 2018c; Dorier et al., 2017). Vieira et al. (2022) showed that pristine and digested E171 can induce DNA damage in intestinal cell lines using both the comet assay and the micronucleus test (Vieira et al., 2022). Malaise et al. (2023) showed an increased number of foci in the nuclei in a murine endothelial monolayer model with the yH2AX assay (Malaise et al., 2024).

We also investigated transcriptional changes in colon organoids following a 24-h exposure to E171 via bulk RNA sequencing. Differential gene expression analysis showed 13 and 110 DEGs at 100 and 250 μg/mL of E171 exposure, compared to control organoids. Our physicochemical characterization of E171 showed that E171 at the dose group of 1000 μg/mL displayed a hydrodynamic diameter twice as large as the lower concentrations. This might be related to the high concentration of E171 in the stock solution, which exceeded the recommended maximum concentration as suggested in the NanoGenoTox dispersion protocol (Jensen et al., 2011). The increase in aggregation size potentially reduced the bioavailability of E171 at 1000 μg/mL, resulting in 0 DEGs with statistical significance. Exposure to such high in vitro doses of E171 generally does not reflect the human situation but helps to compare the results to existing data in the literature and provides insights into physicochemical particle characteristics. Increased particle concentration did not allow for a stable distribution of the particles, as indicated by an increasing aggregation size via DLS. However, increased aggregation size could not be further proven by spICP-MS (Helsper et al., 2016; Frank et al., 2020; Mech et al., 2020). The discrepancies between the results from the DLS measurements and the analysis of the particle/aggregate size via spICP-MS might be related to the different methodological approaches (Helsper et al., 2016). DLS measures the HD, making it more sensitive for aggregates, while spICP-MS measures the core of the particles, which makes it less sensitive for aggregates, since those potentially sediment during the sample preparation process, especially at high concentrations, the likelihood of maintaining aggregates in the dispersion decreases (Helsper et al., 2016; Frank et al., 2020; Mech et al., 2020). On the other hand, the PDIs of the DLS measurements all displayed values that indicated a stable dispersion (PDI <0.2) and, therefore, can be considered relevant (Helsper et al., 2016; Mech et al., 2020). While the effect of increased E171 aggregates did not show an effect on ROS formation or DNA damage, it reduced the effect of E171 on gene expression at 1000 μg/mL, potentially due to reduced bioavailability.

Following DEG analysis, we performed an enrichment pathway analysis, showing pathway alteration related to ribosomal activity and translation at 100 and 250 μg/mL of E171. We found enriched pathways indicative of DNA damage repair and correction mechanisms for faulty RNA, underscoring the coherence between increased DNA damage, as shown in the comet assay, and transcriptional response in the cells related to DNA/RNA damage. Interestingly, we also found pathways related to the Ras/Rab superfamily involving G-protein-coupled receptor (GPCR) signaling. Modulations of GPCR signaling pathways have consistently been reported following E171 exposure in RNA sequencing and microarray experiments in vivo and in vitro (Proquin et al., *2018a;* Proquin et al., *2018b;* Bischoff et al., *2022;* Proquin et al., *2018d)*. We additionally found dysregulation in the Notch signaling pathway with the downregulation of the JAG1 gene, which is crucial in colorectal cancer development (Dai et al., 2014). We detected pathways that indicate the presence of DNA damage, as well as potential mechanisms linking the exposure of E171 to the development of colorectal lesions.

We also performed a GSEA to obtain further insights into the potential molecular mode of action of E171. GSEA depends on ranking the genes, which are analyzed and clustered into gene sets, assessing potential enrichments of said sets according to their stat-value in gene expression, which is a measure for effect size (log2foldchange) and set size (standard error). This approach allows the detection of sets of collectively enriched genes without displaying strong individual changes in those genes.

Our analysis also showed the most potent response of gene expression changes at 250 μg/mL of E171, with activated gene sets that include ribosome, metabolic pathways, oxidative phosphorylation, chemical carcinogenesis – reactive oxygen species, peroxisome, diabetic cardiomyopathy, carbon metabolism, PPAR signaling, and glycolysis/gluconeogenesis.

GSEA analysis showed a consistent activation of ribosome pathways, indicating transcriptional changes toward increased protein synthesis, cell growth, proliferation, and protein metabolism (Jiao et al., 2023; Nait Slimane et al., 2020). The activation of the ribosome pathway, in combination with pathways relating to increased metabolic activity, suggests an elevated need for energy, highlighting amplified cell proliferation and growth (Jiao et al., 2023; Nait Slimane et al., 2020). Several mouse models have reported increased proliferation and hyperplasia of colonic tissue following E171 exposure, including a transgenic mouse model (Urrutia-Ortega et al., 2016; Bischoff et al., 2022; Medina-Reyes et al., 2020). An additional increase in oxidative phosphorylation, peroxisome activity, and glycolysis/gluconeogenesis demonstrates the colon tissue's increased energy demand in the presence of E171. The reprogramming of the cell's metabolism from the citric acid cycle to glycolysis and carbon metabolism, also referred to as the Warburg effect, is a hallmark of cancer and crucial to sustaining infinite proliferation and cell growth (Hanahan, 2022). Furthermore, the accumulation of metabolic waste and a lack of nutrients can influence nearby non-tumor cells and inhibit their survival (Zhong et al., 2022).

CRC often displays dysregulation in their ribosome biogenesis, mainly when arising from chronic ulcerative disease, exhibiting an upregulation of rDNA transcriptional activity (Brighenti et al., 2014). PPAR signaling activation has also been linked to cancer cell proliferation, survival, and apoptosis and has been shown to be upregulated in inflammatory bowel disease and ulcerative colitis patients (Asgharzadeh et al., 2024; Annese et al., 2012). Alteration of other crucial signaling pathways, such as the PI3K-Akt-mTOR pathway, was linked to downstream events following PPAR-beta activation (Asgharzadeh et al., 2024; Leiphrakpam and Are, 2024). PI3K-Akt-mTor pathways are also related to increased glycolysis and altered lipid metabolism, which in vivo contributed to tumor growth, invasion, and metastasis, highlighting the critical role of gene expression associated with these signaling pathways (Asgharzadeh et al., 2024; Leiphrakpam and Are, 2024; Chen et al., 2024). The activation of the translation, Warburg effects, and PPAR suggest a significant upregulation of genes that drive a metabolic shift toward glycolysis. Metabolic reprogramming of cells is often associated with increased cell proliferation, which can contribute to hyperplasia, and indicate potential malignancy in the colon cells (Hanahan, 2022; Zhong et al., 2022).

Huang et al. (2015) indicated an upregulation of HIF-1 signaling genes, which are essential factors in the signaling of the Warburg effect and carbon metabolism, following the in vitro exposure to nano-TiO_2, arguably due to increased formation of ROS (Huang et al., 2015). On the other hand, Kulthong et al. (2022) used a dynamic Caco-2 flow cell model to analyze the effects of E171 in vitro. They reported a downregulation of HIF-1 signaling and glycolysis-related pathways, which stands in contrast with our findings (Kulthong et al., 2021).

Gene sets that showed a suppression following 250 or 1000 μg/mL E171 exposure included ECM-receptor interaction, human papillomavirus infection, signaling pathways regulating pluripotency in stem cells, hippo signaling, PIE3K-Akt signaling pathway, pathways in cancers, focal adhesion, thyroid hormone signaling pathway, Wnt signaling pathway, regulation of actin cytoskeleton, PD-L1 expression and PD-1 checkpoint pathway in cancer, efferocytosis, growth hormone synthesis, and hedgehog signaling. ECM receptor interaction, actin cytoskeleton regulation, and focal adhesion are crucial in maintaining healthy tissue organization and cell function (Zucker and Vacirca, 2004; Filou et al., 2015). Disruption of their function is commonly seen in CRC and is the foundation of successful metastasis, particularly prominent in CRC

(Zucker and Vacirca, 2004; Filou et al., 2015; Ii et al., 2006). ECM provides structural support to tissue and helps to regulate cellular behavior via integrins. The suppression of ECM receptor interaction might mitigate cell adhesion and increase tissue disorganization, characterized as a hallmark of cancer, due to its facilitation of tumor progression, increased cancer cell invasion, and metastasis (Hanahan, 2022; Filou et al., 2015; Ii et al., 2006). Focal adhesion links ECM to the cytoskeleton, transmits signals from the extracellular space to the intracellular space, and regulates cell survival, growth, and motility (Kanchanawong and Calderwood, 2023). Suppression of the focal adhesion pathway can weaken overall cellular architecture and might activate PI3K-Akt or mTor pathways, further promoting tumor progression (Paul et al., 2020).

Suppression of signaling pathways included MAPK, Hippo signaling, PI3K-Akt signaling pathway, pathways in cancer, Wnt signaling, and PD-L1 expression and PD-1 checkpoint pathway in cancer, revealed a distinct pattern following the exposure to 250 or 1000 μg/mL E171. WNT signaling, a key player in colorectal cancer, through its modification and degradation of beta-catenin, has also been modulated in our experiment, showing yet another association between E171 exposure and CRC development. TiO_2, especially in its nanoparticle form, has shown the potential to alter WNT signaling in different animal and cell models (Proquin et al., 2018b; Liu et al., 2017; Yu et al., 2020; Hong et al., 2017). Wnt cross-talk with Hippo signaling is important in maintaining organ size and cell proliferation by regulating apoptosis and inhibiting excessive cell growth (Fu et al., 2024). Suppression of Hippo signaling can lead to unregulated cell growth and potential tumor formation (Fu et al., 2024). PI3K-Akt signaling is a critical regulator of metabolism, growth, and survival, which supports epithelial cell survival and protects against apoptosis in stress response (Leiphrakpam and Are, 2024). Its interplay with PD-L1 expression is an important regulator for the immune system (Chung et al., 2022).

These crucial pathways in the development of CRC are usually upregulated, while our findings indicate suppression of pathways and genes. However, our analysis showed that Axin 1 and Axin 2 were strongly suppressed in the Wnt signaling pathways. Axin1 and Axin 2 function as inhibitors for beta-catenin production. Inhibition of Axin 1 and 2 increases beta-catenin and leads to activation of cell proliferation. The suppression of, e.g., the WNT signaling pathway might be due to the short-lived exposure of only 24 h and compensatory cellular mechanisms, which try to counteract the activation of the Wnt pathways. This initial stress phase still indicates potential genes and mechanisms involved in the adversity of E171 exposure and represents an acute response. Prolonged exposure times might help better understand and crystalize the underlying mechanism and assist in the hazard characterization of E171 in colon organoids.

While our use of human iPSC-derived colon organoids provides a significant advancement in modeling E171 toxicity, there are some limitations to consider. Despite their improved complexity as compared to 2D models, organoids do not fully replicate the entire human gastrointestinal environment. Factors such as gut microbiota interactions, immune responses, and systemic metabolism cannot be entirely modeled in vitro. Additionally, while relevant for short-term toxicity assessments, this study's exposure concentrations and durations do also not represent chronic exposure scenarios typically experienced through dietary intake. Further considerations, particularly regarding our experimental setup, are related to the insolubility of E171 in combination with a physical barrier around the colon organoids in the form of matrigel. The matrigel barrier makes an accurate dose prediction difficult. It limits the direct interaction of E171 with the colonic tissue, potentially underestimating the effect E171 has on the cells due to restricting their physical interaction. This is important since the physical interaction of E171 with the colonic tissue has been postulated as the primary mechanism, inducing adverse effects (Bischoff et al., 2020).

This study is among the first to employ human iPSC-derived colon organoids to assess the toxicological effects of E171. Unlike traditional 2D cell cultures and animal models, these 3D organoids offer a more physiologically relevant model that closely mimics human intestinal tissue and provides a helpful tool to advance the field of toxicology and, in particular, nanotoxicology (Kim et al., 2020; Nikonorova et al., 2023; Taelman et al., 2022). Integrating a standardized RNA-seq processing pipeline in this model further enhances our understanding of the molecular mechanisms driving E171 toxicity. It highlights potential biomolecular processes contributing to E171-induced adverse events and its mode of action.

5. Conclusion

In conclusion, this study showed the potential toxicity of E171 using human iPSC-derived colon organoids. Our results indicate that E171 exposure leads to a statistically significant increase in ROS. We observed increased DNA damage in both the standard and FPG alkaline comet assays, highlighting the genotoxic potential of E171 and its correlation with increased oxidative stress. Furthermore, RNA sequencing and subsequent pathway analysis showed that E171 significantly alters the expression of genes involved in signal transduction, DNA damage/repair, and metabolic pathways. Activated pathways included ribosome function and a metabolic shift in colon cells, indicating the Warburg effect. We also detected suppression of pathways related to ECM modulation, Wnt signaling, PI3K signaling, and cancer-related PD-L1/PD-1 checkpoint pathways. These findings suggest a potential mode of action in which E171 induces oxidative stress and DNA damage, triggering cancer-related gene expression changes related to several cancer hallmarks.

The implications of this study extend beyond the immediate effects of E171 on colon organoids. Given the widespread use of E171 in food products and its potential health risks, our findings contribute to the growing body of evidence that questions the safety of E171. The observed modulations of gene expression and pathways align with previous animal studies and raise concerns about the long-term effects of E171 consumption on human CRC risk. Our results support the recent regulatory decisions in the EU to ban E171 as a food additive, underscoring the need for further research into its long-term health implications.

CRediT authorship contribution statement

Nicolaj S. Bischoff: Writing – review & editing, Writing – original draft, Visualization, Validation, Methodology, Data curation, Conceptualization. **Anna K. Undas:** Writing – review & editing, Visualization, Methodology. **Marcel van Herwijnen:** Writing – review & editing, Methodology. **Marcha Verheijen:** Writing – review & editing, Software, Methodology, Data curation. **Jacco J. Briedé:** Writing – review & editing, Supervision, Methodology, Conceptualization. **Simone G. van Breda:** Writing – review & editing, Supervision, Methodology, Conceptualization. **Dick T.H.M. Sijm:** Writing – review & editing, Supervision, Project administration, Methodology, Conceptualization. **Theo M. de Kok:** Writing – review & editing, Supervision, Methodology, Conceptualization.

Funding

Maastricht University, Netherlands: internal funding, Nederlandse Voedsel- en Warenautoriteit (NVWA), Netherlands: ARVODI-2018 Overeenkomst Onderzoeksopdracht E171.

Declaration of competing interest

The authors declare no potential conflict to this article's research, authorship, and publication.

Acknowledgment

We thank Yueqin He for her invaluable assistance and expertise in setting up and establishing the organoid cell culture. We also sincerely thank Florian Caiment for his insightful guidance in designing and implementing the RNA sequencing experiments and his support during the data analysis process.

Appendix A. Supplementary data

Supplementary data to this article can be found online at https://doi.org/10.1016/j.tiv.2025.106105.

Data availability

The RNA sequencing fastq files will be made available on 01.05.2025 under the accession number E-MTAB-147888 on https://www.ebi.ac.uk/biostudies/arrayexpress/studies/E-MTAB-14778

References

Annese, V., Rogai, F., Settesoldi, A., Bagnoli, S., 2012. PPARgamma in inflammatory bowel disease. PPAR Res. 2012, 620839.
Asgharzadeh, F., Memarzia, A., Alikhani, V., Beigoli, S., Boskabady, M.H., 2024. Peroxisome proliferator-activated receptors: key regulators of tumor progression and growth. Transl. Oncol. 47, 102039.
Augustyniak, J., Bertero, A., Coccini, T., Baderna, D., Buzanska, L., Caloni, F., 2019. Organoids are promising tools for species-specific in vitro toxicological studies. J. Appl. Toxicol. 39 (12), 1610–1622.
Bettencourt, A., Goncalves, L.M., Gramacho, A.C., Vieira, A., Rolo, D., Martins, C., et al., 2020. Analysis of the characteristics and cytotoxicity of titanium dioxide nanomaterials following simulated in vitro digestion. Nanomaterials (Basel) 10 (8).
Bettini, S., Boutet-Robinet, E., Cartier, C., Comera, C., Gaultier, E., Dupuy, J., et al., 2017. Food-grade TiO2 impairs intestinal and systemic immune homeostasis, initiates preneoplastic lesions and promotes aberrant crypt development in the rat colon. Sci. Rep. 7, 40373.
Bischoff, N.S., de Kok, T.M., Sijm, D., van Breda, S.G., Briede, J.J., Castenmiller, J.J.M., et al., 2020. Possible adverse effects of food additive E171 (titanium dioxide) related to particle specific human toxicity, including the immune system. Int. J. Mol. Sci. 22 (1).
Bischoff, N.S., Proquin, H., Jetten, M.J., Schrooders, Y., Jonkhout, M.C.M., Briedé, J.J., et al., 2022. The effects of the food additive titanium dioxide (E171) on tumor formation and gene expression in the colon of a transgenic mouse model for colorectal cancer. Nanomaterials-Basel. 12 (8).
Bischoff, N.S., Undas, A.K., van Bemmel, G., Briede, J.J., van Breda, S.G., Verhoeven, J., et al., 2024. Investigating the ROS formation and particle behavior of food-grade titanium dioxide (E171) in the TIM-1 dynamic gastrointestinal digestion model. Nanomaterials (Basel) 15 (1).
Blevins, L.K., Crawford, R.B., Bach, A., Rizzo, M.D., Zhou, J., Henriquez, J.E., et al., 2019. Evaluation of immunologic and intestinal effects in rats administered an E 171-containing diet, a food grade titanium dioxide (TiO2). Food Chem. Toxicol. 133, 110793.
Botelho, M.C., Costa, C., Silva, S., Costa, S., Dhawan, A., Oliveira, P.A., et al., 2014. Effects of titanium dioxide nanoparticles in human gastric epithelial cells in vitro. Biomed. Pharmacother. 68 (1), 59–64.
Brighenti, E., Calabrese, C., Liguori, G., Giannone, F.A., Trerè, D., Montanaro, L., et al., 2014. Interleukin 6 downregulates p53 expression and activity by stimulating ribosome biogenesis: a new pathway connecting inflammation to cancer. Oncogene 33 (35), 4396–4406.
Canada, H., 2023. Titanium Dioxide (TiO2) as a Food Additive: Current Science Report.
Chen, X., Ma, Z., Yi, Z., Wu, E., Shang, Z., Tuo, B., et al., 2024. The effects of metabolism on the immune microenvironment in colorectal cancer. Cell Death Dis. 10 (1), 118.
Chung, B.S., Liao, I.C., Lin, P.C., Wu, S.Y., Kang, J.W., Lin, B.W., et al., 2022. PD-L1 expression in high-risk early-stage colorectal cancer-its clinical and biological significance in immune microenvironment. Int. J. Mol. Sci. 23 (21).
Collins, A., Moller, P., Gajski, G., Vodenková, S., Abdulwahed, A., Anderson, D., et al., 2023. Measuring DNA modifications with the comet assay: a compendium of protocols. Nat. Protoc. 18 (3), 929–989.
Dai, Y., Wilson, G., Huang, B., Peng, M., Teng, G., Zhang, D., et al., 2014. Silencing of Jagged1 inhibits cell growth and invasion in colorectal cancer. Cell Death Dis. 5 (4), e1170.
David, O.M., Lategan, K.L., de Cortalezzi, M.F., Pool, E.J., 2022. The stability and anti-angiogenic properties of titanium dioxide nanoparticles (TiO(2)NPs) using Caco-2 cells. Biomolecules 12 (10).
Dorier, M., Beal, D., Marie-Desvergne, C., Dubosson, M., Barreau, F., Houdeau, E., et al., 2017. Continuous in vitro exposure of intestinal epithelial cells to E171 food additive causes oxidative stress, inducing oxidation of DNA bases but no endoplasmic reticulum stress. Nanotoxicology 11 (6), 751–761.
Dorier, M., Tisseyre, C., Dussert, F., Beal, D., Arnal, M.E., Douki, T., et al., 2019. Toxicological impact of acute exposure to E171 food additive and TiO2 nanoparticles on a co-culture of Caco-2 and HT29-MTX intestinal cells. Mutat. Res. 845, 402980.
Dudefoi, W., Rabesona, H., Rivard, C., Mercier-Bonin, M., Humbert, B., Terrisse, H., et al., 2021. In vitro digestion of food grade TiO2 (E171) and TiO2 nanoparticles: physicochemical characterization and impact on the activity of digestive enzymes. Food Funct. 12 (13), 5975–5988.
Dvoranova, D., Barbierikova, Z., Brezova, V., 2014. Radical intermediates in photoinduced reactions on TiO2 (an EPR spin trapping study). Molecules 19 (11), 17279–17304.
EEA, 2022. Commission Regulation (EU) 2022/63 of 14 January 2022 amending Annexes II and III to Regulation (EC) No 1333/2008 of the European Parliament and of the Council as regards the food additive titanium dioxide (E 171) (Text with EEA relevance). Official Journal of the European Unon. 18.01.2022;L11/1.
Ferrante, M., Grasso, A., Salemi, R., Libra, M., Tomasello, B., Fiore, M., et al., 2023. DNA damage and apoptosis as in-vitro effect biomarkers of titanium dioxide nanoparticles (TiO(2)-NPs) and the food additive E171 toxicity in colon cancer cells: HCT-116 and Caco-2. Int. J. Environ. Res. Public Health 20 (3).
Filou, S., Korpetinou, A., Kyriakopoulou, D., Bounias, D., Stavropoulos, M., Ravazoula, P., et al., 2015. ADAMTS expression in colorectal cancer. PLoS One 10 (3), e0121209.
Frank, Mech A.B., Hodoroaba, Vasile-Dan, Ghane, Antoine M., Wohlleben, Wendel, Marvin, Hans, Löschner, Katrin, Brüngel, Raphael, Friedrich, Christoph M., 2020. The NanoDefine Methods Manual. Part 3: Standard Operating Procedures (SOPs) JRC117501. DTU Library.
Fu, M.Y., Hu, Y., Lan, T.X., Guan, K.L., Luo, T., Luo, M., 2024. The Hippo signalling pathway and its implications in human health and diseases (vol 7, 376, 2022). Signal Transduct. Tar. 9 (1).
Guo, Z.Y., Martucci, N.J., Moreno-Olivas, F., Tako, E., Mahler, G.J., 2017. Titanium dioxide nanoparticle ingestion alters nutrient absorption in an model of the small intestine. Nanoimpact 5, 70–82.
Hanahan, D., 2022. Hallmarks of cancer: new dimensions. Cancer Discov. 12 (1), 31–46.
Helsper, J.P., Peters, R.J., van Bemmel, M.E., Rivera, Z.E., Wagner, S., von der Kammer, F., et al., 2016. Physicochemical characterization of titanium dioxide pigments using various techniques for size determination and asymmetric flow field flow fractionation hyphenated with inductively coupled plasma mass spectrometry. Anal. Bioanal. Chem. 408 (24), 6679–6691.
Hong, F., Ze, Y.A., Zhou, Y.M., Hong, J., Yu, X.H., Sheng, L., et al., 2017. Nanoparticulate TiO -mediated inhibition of the Wnt signaling pathway causes dendritic development disorder in cultured rat hippocampal neurons. J. Biomed. Mater. Res. A 105 (8), 2139–2149.
Huang, K.T., Wu, C.T., Huang, K.H., Lin, W.C., Chen, C.M., Guan, S.S., et al., 2015. Titanium nanoparticle inhalation induces renal fibrosis in mice via an oxidative stress upregulated transforming growth factor-beta pathway. Chem. Res. Toxicol. 28 (3), 354–364.
Hubrecht, R.C., Carter, E., 2019. The 3Rs and humane experimental technique: implementing change. Animals (Basel) 9 (10).
Ii, M., Yamamoto, H., Adachi, Y., Maruyama, Y., Shinomura, Y., 2006. Role of matrix metalloproteinase-7 (matrilysin) in human cancer invasion, apoptosis, growth, and angiogenesis. Exp. Biol. Med. (Maywood) 231 (1), 20–27.
Jensen, K., Kembouche, Y., Christiansen, E., Jacobsen, N., Wallin, H., Guiot, C., et al., 2011. The generic NANOGENOTOX dispersion protocol—standard operation procedure (SOP). In: NANOGENOTOX Deliverable Report, p. 3.
Jiao, L.J., Liu, Y.Z., Yu, X.Y., Pan, X.B., Zhang, Y., Tu, J.C., et al., 2023. Ribosome biogenesis in disease: new players and therapeutic targets. Signal Transduct. Tar. 8 (1).
Kampfer, A.A.M., Busch, M., Buttner, V., Bredeck, G., Stahlmecke, B., Hellack, B., et al., 2021. Model complexity as determining factor for in vitro nanosafety studies: effects of silver and titanium dioxide nanomaterials in intestinal models. Small 17 (15).
Kanchanawong, P., Calderwood, D.A., 2023. Organization, dynamics and mechanoregulation of integrin-mediated cell-ECM adhesions. Nat. Rev. Mol. Cell Biol. 24 (2), 142–161.
Kim, J., Koo, B.K., Knoblich, J.A., 2020. Human organoids: model systems for human biology and medicine. Nat. Rev. Mol. Cell Biol. 21 (10), 571–584.
Kulthong, K., Hooiveld, G.J.E.J., Duivenvoorde, L.P.M., Estruch, I.M., Bouwmeester, H., van der Zande, M., 2021. Comparative study of the transcriptomes of Caco-2 cells cultured under dynamic vs. static conditions following exposure to titanium dioxide and zinc oxide nanomaterials. Nanotoxicology 15 (9), 1233–1252.
Leiphrakpam, P.D., Are, C., 2024. PI3K/Akt/mTOR signaling pathway as a target for colorectal cancer treatment. Int. J. Mol. Sci. 25 (6).
Li, M., Yin, J.J., Wamer, W.G., Lo, Y.M., 2014. Mechanistic characterization of titanium dioxide nanoparticle-induced toxicity using electron spin resonance. J. Food Drug Anal. 22 (1), 76–85.
Liu, C., Li, P., Chen, N., Jiang, Y., Shi, J., Fan, C., et al., 2017. Titanium dioxide nanoparticles trigger non-canonical receptor endocytosis to inhibit Wnt signaling. J. Biomed. Nanotechnol. 13 (11), 1522–1532.
Malaise, Y., Casale, E., Pettes-Duler, A., Cartier, C., Gaultier, E., Martins Breyner, N., et al., 2024. Validating enteroid-derived monolayers from murine gut organoids for toxicological testing of inorganic particles: proof-of-concept with food-grade titanium dioxide. Int. J. Mol. Sci. 25 (5).
Mech, A., Wohlleben, W., Ghanem, A., Hodoroaba, V.D., Weigel, S., Babick, F., et al., 2020. Nano or not nano? A structured approach for identifying nanomaterials according to the European Commission's definition. Small 16 (36), e2002228.
Medina-Reyes, E.I., Delgado-Buenrostro, N.L., Diaz-Urbina, D., Rodriguez-Ibarra, C., Deciga-Alcaraz, A., Gonzalez, M.I., et al., 2020. Food-grade titanium dioxide (E171) induces anxiety, adenomas in colon and goblet cells hyperplasia in a regular diet

model and microvesicular steatosis in a high fat diet model. Food Chem. Toxicol. 146, 111786.
Nait Slimane, S., Marcel, V., Fenouil, T., Catez, F., Saurin, J.C., Bouvet, P., et al., 2020. Ribosome biogenesis alterations in colorectal cancer. Cells 9 (11).
NanoDefine, 2016. Development of an integrated approach based on validated and standardized methods to support the implementation of the EC recommendations for a definition of nanomaterials. FP7-NMP-2013-LARGE(NMP.2013.1.4–3 2013–2016). www.nanodefine.eu.
Nikonorova, V.G., Chrishtop, V.V., Mironov, V.A., Prilepskii, A.Y., 2023. Advantages and potential benefits of using organoids in nanotoxicology. Cells 12 (4).
Park, S.B., Jung, W.H., Kim, K.Y., Koh, B., 2020. Toxicity assessment of SiO2 and TiO2 in normal colon cells, in vivo and in human colon organoids. Molecules 25 (16).
Paul, R., Luo, M., Mo, X.Y., Lu, J., Yeo, S.K., Guan, J.L., 2020. FAK activates AKT-mTOR signaling to promote the growth and progression of MMTV-Wnt1-driven basal-like mammary tumors (vol 22, 59, 2020). Breast Cancer Res. 22 (1).
Proquin, H., Jetten, M.J., Jonkhout, M.C.M., Garduno-Balderas, L.G., Briede, J.J., de Kok, T.M., et al., 2018a. Gene expression profiling in colon of mice exposed to food additive titanium dioxide (E171). Food Chem. Toxicol. 111, 153–165.
Proquin, H., Jetten, M.J., Jonkhout, M.C.M., Garduno-Balderas, L.G., Briede, J.J., de Kok, T.M., et al., 2018b. Transcriptomics analysis reveals new insights in E171-induced molecular alterations in a mouse model of colon cancer. Sci. Rep. 8 (1), 9738.
Proquin, H., Rodriguez-Ibarra, C., Moonen, C., Urrutia Ortega, I.M., Briede, J.J., de Kok, T.M., et al., 2018c. Titanium dioxide food additive (E171) induces ROS formation and genotoxicity: contribution of micro and nano-sized fractions. Mutagenesis 33 (3), 267–268.
Proquin, H., Jetten, M.J., Jonkhout, M.C.M., Garduno-Balderas, L.G., Briede, J.J., de Kok, T.M., et al., 2018d. Time course gene expression data in colon of mice after exposure to food-grade E171. Data Brief 16, 531–600.
Proquin, H., Jonkhout, M.C.M., Jetten, M.J., van Loveren, H., de Kok, T.M., Briede, J.J., 2019. Transcriptome changes in undifferentiated Caco-2 cells exposed to food-grade titanium dioxide (E171): contribution of the nano- and micro- sized particles. Sci. Rep. 9 (1), 18287.
Putra, C., Bello, D., Kelleher, S.L., Tucker, K.L., Mangano, K.M., 2024. Stool titanium dioxide is positively associated with stool alpha-1 antitrypsin and calprotectin in young healthy adults. Nanoimpact 33.
Scheinok, S., Leveque, P., Sonveaux, P., Driesschaert, B., Gallez, B., 2018. Comparison of different methods for measuring the superoxide radical by EPR spectroscopy in buffer, cell lysates and cells. Free Radic. Res. 52 (10), 1182–1196.
Schoonjans, R., Castenmiller, J., Chaudhry, Q., Cubadda, F., Daskaleros, T., Franz, R., et al., 2023. Regulatory safety assessment of nanoparticles for the food chain in Europe. Trends Food Sci. Technol. 130, 98–111.
Taelman, J., Diaz, M., Guiu, J., 2022. Human intestinal organoids: promise and challenge. Front. Cell Dev. Biol. 10, 854740.
Administration USFaD, 2024. Titanium Dioxide as a Color Additive in Foods.
Urrutia-Ortega, I.M., Garduno-Balderas, L.G., Delgado-Buenrostro, N.L., Freyre-Fonseca, V., Flores-Flores, J.O., Gonzalez-Robles, A., et al., 2016. Food-grade titanium dioxide exposure exacerbates tumor formation in colitis associated cancer model. Food Chem. Toxicol. 93, 20–31.
Vedi, M., Nalabolu, H.S., Lin, C.W., Hoffman, M.J., Smith, J.R., Brodie, K., et al., 2022. MOET: a web-based gene set enrichment too at the rat genome database for multiontology and multispecies analyses. Genetics 220 (4).
Verheijen, M., Meier, M.J., Ochoteco, J., Gant, T.W., Tong, W., Yauk, C.L., et al., 2022. R-ODAF: an omics data analysis framework for regulatory application. Toxicol. Lett. 368. S253-S.
Verleysen, E., Waegeneers, N., Brassinne, F., De Vos, S., Jimenez, I.O., Mathioudaki, S., et al., 2020. Physicochemical characterization of the pristine E171 food additive by standardized and validated methods. Nanomaterials (Basel) 10 (3).
Vieira, A., Vital, N., Rolo, D., Roque, R., Goncalves, L.M., Bettencourt, A., et al., 2022. Investigation of the genotoxicity of digested titanium dioxide nanomaterials in human intestinal cells. Food Chem. Toxicol. 161, 112841.
Vigneshwaran, R., Ezhilarasan, D., Rajeshkumar, S., 2021. Inorganic titanium dioxide nanoparticles induces cytotoxicity in colon cancer cells. Inorg. Chem. Commun. 133.
Weir, A., Westerhoff, P., Fabricius, L., Hristovski, K., von Goetz, N., 2012. Titanium dioxide nanoparticles in food and personal care products. Environ. Sci. Technol. 46 (4), 2242–2250.
Winkler, H.C., Notter, T., Meyer, U., Naegeli, H., 2018. Critical review of the safety assessment of titanium dioxide additives in food. J. Nanobiotechnol. 16 (1), 51.
Wu, T., Hu, E., Xu, S., Chen, M., Guo, P., Dai, Z., et al., 2021. clusterProfiler 4.0: a universal enrichment tool for interpreting omics data. Innovation (Camb) 2 (3), 100141.
Younes, M., Aquilina, G., Castle, L., Engel, K.H., Fowler, P., Fernandez, M.J.F., et al., 2021. Safety assessment of titanium dioxide (E171) as a food additive. EFSA J. 19 (5).
Yu, G., Wang, L.G., Han, Y., He, Q.Y., 2012. clusterProfiler: an R package for comparing biological themes among gene clusters. OMICS 16 (5), 284–287.
Yu, S., Wang, F., Bi, Y., Wang, P., Zhang, R., Bohatko-Naismith, J., et al., 2020. Autophagy regulates the Wnt/GSK3beta/beta-catenin/cyclin D1 pathway in mesenchymal stem cells (MSCs) exposed to titanium dioxide nanoparticles (TiO(2) NPs). Toxicol. Rep. 7, 1216–1222.
Zhong, X., He, X., Wang, Y., Hu, Z., Huang, H., Zhao, S., et al., 2022. Warburg effect in colorectal cancer: the emerging roles in tumor microenvironment and therapeutic implications. J. Hematol. Oncol. 15 (1), 160.
Zucker, S., Vacirca, J., 2004. Role of matrix metalloproteinases (MMPs) in colorectal cancer. Cancer Metastasis Rev. 23 (1–2), 101–117.